applied optics

High-efficiency quantum dot remote phosphor film

Qi Hong,[1] Kuo-Chang Lee,[2] Zhenyue Luo,[1] and Shin-Tson Wu[1,*]

[1]CREOL, The College of Optics and Photonics, University of Central Florida, Orlando, Florida 32816, USA
[2]Display Technology Center, Industrial Technology Research Institute, Chutung, Hsinchu 31040, Taiwan
*Corresponding author: swu@ucf.edu

Received 13 January 2015; revised 11 April 2015; accepted 16 April 2015; posted 17 April 2015 (Doc. ID 232339); published 11 May 2015

We report a high-efficiency quantum dot (QD) film for high color gamut edge-lit LCD backlights. On the film's input surface, an array of asymmetric microprisms is used to preserve the large off-axis angle of the incident blue light. On the exit surface, the retroreflective microprisms retain blue light inside the film. The extended optical path effectively enhances the blue light's probability to hit QDs and generate downconverted wavelengths. When not using any volume scattering particles, fewer QDs are needed to re-emit higher power green and red light, which helps lower the material cost.

OCIS codes: (250.5230) Photoluminescence; (250.5590) Quantum-well, -wire and -dot devices; (160.2540) Fluorescent and luminescent materials; (330.1715) Color, rendering and metamerism; (230.3720) Liquid-crystal devices.

http://dx.doi.org/10.1364/AO.54.004617

1. INTRODUCTION

Quantum dot (QD) backlights provide a promising solution to widen the color gamut of liquid crystal displays (LCDs) [1–5]. The narrow emission spectrum enables vivid colors and reduces crosstalk between colors [4–10]. Unlike a QD LED, which encapsulates quantum dots into an LED package, remote phosphor QD film disperses quantum dots inside an optical film to avoid high operating temperature and high light flux, which in turn yields higher efficiency and longer lifetime [2].

Quantum dot diffuser film has been developed for edge-lit LCD backlights [2]. A QD diffuser film consists of a quantum dot layer sandwiched between two substrates. Green and red quantum dots as well as light scattering particles are uniformly suspended in the matrix to form the QD layer. The incident blue light is downconverted by green and red quantum dots to longer wavelengths. Inside the QD layer, light scattering particles increase the incident light path length to enhance the downconversion efficiency. On the surfaces of top and bottom substrates, diffusive surface features scatter the re-emitted light and improve the extraction efficiency. Such a diffusive surface feature usually has random sizes and shapes.

In this paper, we propose a high efficiency quantum dot prism film that requires fewer quantum dots to re-emit higher power green and red light, without the need for any volume scattering particles. The optical path of the incident blue light is extended by an array of asymmetric microprisms on the input surface of the bottom substrate. Retroreflective microprism arrays on the exit surface of the top substrate retain more blue light inside the film to further enhance light conversion. Meanwhile, the proposed surface features allow re-emitted light to exit the QD film beyond the light emission cone. With more light conversion and better light extraction, a smaller quantity of QD material could re-emit higher power light. In addition, much lower volume density reduces QD's tendency to aggregate, so that the QD film's optical efficiency can be further improved [11,12]. The replication process of microprism surface features is similar to the manufacturing of diffusive surface features. Currently, low-cost microprism films are very common in LCD backlights.

2. QD DIFFUSER FILM

In an edge-lit LCD backlight, a QD diffuser film can be inserted between a light guide plate (LGP) and light recycling films, as Fig. 1 illustrates [2]. Green and red QDs are uniformly suspended in the matrix and sandwiched between the top and bottom substrates. The excitation light is coming from the blue LED. The LGP uniformly spreads out the blue light over the entire backlight. Entering the QD film, a portion of the blue light is absorbed after hitting QDs, then downconverted and re-emitted as green and red. The remaining blue light passes through and reaches the light-recycling-type brightness enhancement films (BEFs). Light recycling films collimate and recycle all the light to improve on-axis gain. The light recycling process also allows blue light to pass through the QD film several times, so that the possibility of downconversion is higher and the overall optical efficiency can be improved.

The optical efficiency of such a QD film depends on not only the QD materials but also the utilization of incident blue

light. Recent advances in QD sciences have led to nearly 100% quantum efficiency [13–19], while downconversion occurs only when the excitation light hits QD particles. The probability of hitting a QD particle depends on two factors: the QD particle density and the blue light path length. Currently, the high cost of QD material limits the quantity to be used. Another limiting factor is QD's secondary absorption of the re-emitted light, which is caused by the partial overlapping between QD's absorption and emission spectra. Furthermore, closely packed QD particles tend to cluster into domains and lower the optical efficiency [11,12]. Increasing the QD particle density does not guarantee a higher power output. On the other hand, if the incident light travels a longer distance inside the QD layer, it is more likely to hit a QD particle, even if the particle density is not too high.

Light scattering is a common approach to extend the pumping light's path length. Since QD particle radius is much smaller than the pumping blue wavelength, scattering is insignificant. Blending additional scattering particles into the QD film is necessary. Scattering particles randomly change the input light's traveling direction several times before it exits the QD film, which extends the path length and increases the possibility of hitting QDs. However, the re-emitted light also changes direction after hitting a scattering particle. The possibility of hitting other QDs and being partially absorbed is also increased for the re-emitted beam. A higher particle density of neither QD nor scattering particle helps.

Here, we used the ray-tracing software LightTools to evaluate the QD film's light conversion. The QD photoluminescence is simulated using LightTools Advanced Physics Module. As depicted in Fig. 1, QD film is sandwiched between the LGP and crossed BEFs. The substrate and QD matrix are assumed to be polymethyl methacrylate (PMMA). Beneath the LGP is a white reflector having 98% reflectance: 92% of the reflection is diffusive and the remaining 8% is near specular. The edge-lit blue LED array serves as excitation beam for green and red QDs. The unconverted blue light illuminates the LCD's blue pixels. The LGP is designed such that the illuminance is uniform across the entire plate and the luminous intensity peaks at 70° off-axis, as Fig. 2 shows.

Figure 3(a) depicts the measured absorption spectra of two QD samples purchased from Cytodiagnostics [5]. The samples were measured using a Varian Cary 500 Scan UV–Vis

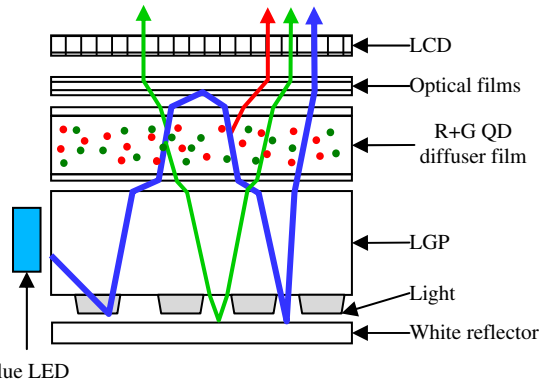

Fig. 1. LCD backlight using conventional diffusive QD film.

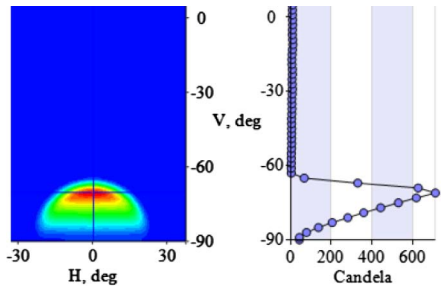

Fig. 2. Light guide plate's luminous intensity distribution.

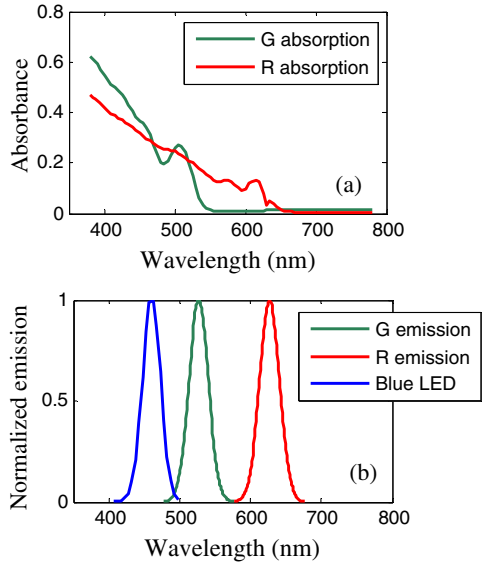

Fig. 3. (a) Measured absorption spectra of the green and red QD materials, and (b) normalized emission spectra of green and red QDs when pumped by a blue InGaN LED with peak wavelength at $\lambda = 459$ nm.

Spectrometer. The QD materials have a core–shell structure, with CdS_xSe_{1-x} as the core and ZnS as the shell. The particle size is between 5.5 and 6.5 nm so that the light scattering caused by QDs is negligible in our simulations. Depending on the composition ratio x of the core material, our QD samples emit green or red light with high purity when excited by a blue InGaN LED ($\lambda = 459$ nm), which is shown in Fig. 3(b). Comparing Figs. 3(a) and 3(b) we can see the partial overlapping between absorption and emission spectra, which causes secondary absorption when the re-emitted light hits other QD particles.

Because of the QD's isotropic emission pattern, total internal reflection (TIR) on the two parallel surfaces would trap a significant amount of re-emitted light inside the QD film if the input and the exit surfaces were planar. Surface scatterings on the top and bottom surfaces help light extractions while increasing the incident light's average path length inside the QD layer. In our simulations, we use Gaussian scattering to approximate the light distribution caused by surface scattering [20]. The intensity distribution is given by

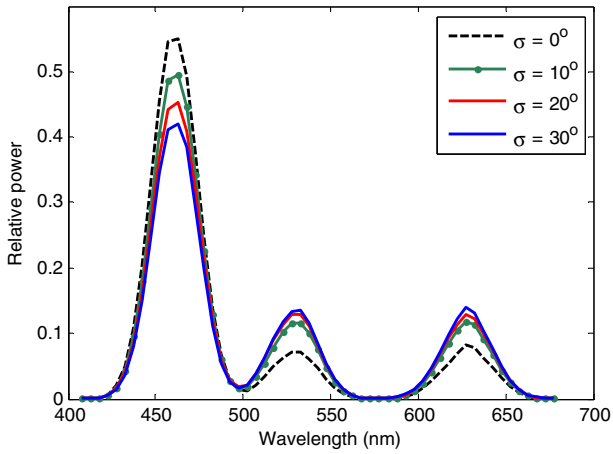

Fig. 4. Stronger surface scattering increases light conversion and improves light extraction. Spectral power distributions are normalized by the incident light's power at $\lambda = 459$ nm. Green QD $MFP_g = 1.4$ mm, red QD $MFP_r = 1.7$ mm, and scattering particle density is $N_s = 10^6/\text{mm}^3$. QD layer thickness = 200 μm.

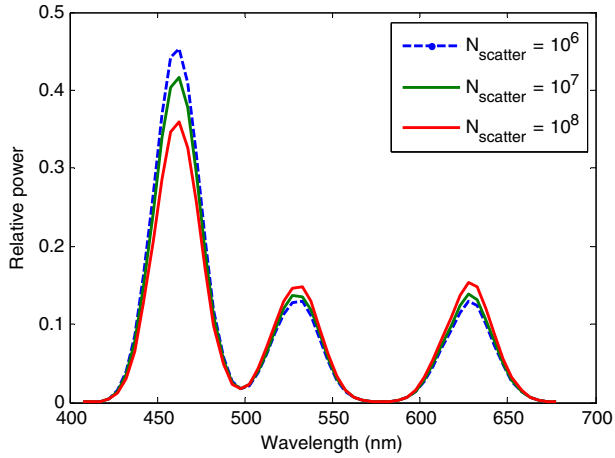

Fig. 5. Relative power spectra at different scattering particle densities. Here $MFP_g = 1.4$ mm, and $MFP_r = 1.7$ mm. Gaussian scattering $\sigma = 20°$. QD layer thickness = 200 μm.

$$P(\theta) = P_o \cdot \exp\left[\left(-\frac{1}{2}\right) \cdot \left(\frac{\theta}{\sigma}\right)^2\right], \quad (1)$$

where $P(\theta)$ is the intensity at angle θ, P_o is the intensity at the specular direction, and σ is the standard deviation of Gaussian distribution. To improve light conversion efficiency, the QD layer contains scattering particles with radius of 500 nm and refractive index of 1.75. QDs are defined as phosphor particles in LightTools simulations. The absorption spectrum, emission property, and reabsorption are all taken into account during calculations. The QD mean free path (MFP) is inversely proportional to the particle density [20,21]:

$$\text{MFP} = \frac{1}{N \times a_{\text{eff}}}, \quad (2)$$

where N is the particle density, and α_{eff} is the effective cross-section area. Therefore, the ratio between two particle densities is inversely proportional to the ratio between their MFPs, which is $N_2/N_1 = \text{MFP}_1/\text{MFP}_2$. The receiver is located after the crossed BEFs so that our simulation also considers the light recycling effect, which causes a portion of the incident and re-emitted lights to pass through the QD film several times.

We used the incident blue light peak power to normalize the QD film's output spectra. Figure 4 compares the effects of surface scattering on light conversion. Without surface scattering, after absorption and downconversion, the blue light's peak power remains 0.55 of the incident's peak, while the peak powers of re-emitted green and red light are only about 0.07–0.08 of the input. With Gaussian scattering $\sigma = 10°$, the blue light's relative peak power drops to 0.496, while both green and red light jump to 0.12. Surface scatterings on the top and bottom substrates effectively increase the blue light path length and help the light extraction. This trend continues when σ is further increased to 20° and 30°, although re-emission is not improved significantly. Here we assume green QD $MFP_g = 1.4$ mm and red QD $MFP_r = 1.7$ mm [21]. Scattering particle density $N_s = 10^6/\text{mm}^3$, which is equivalent to $MFP_s = 0.37$ mm at $\lambda = 459$ nm, according to LightTools' estimation using Mie theory [20,21].

Adding more scattering particles to the QD layer can also enhance light conversion. Figure 5 shows the relative power spectra at different scattering particle densities. Adding more scattering particles significantly increases the blue light absorption but only slightly increases the output of green and red light. A large portion of the re-emitted light is lost during multiple scattering. Therefore, high density of a light scattering particle can result in only limited improvement, but increase the material cost.

3. HIGH-EFFICIENCY QD PRISM FILM

Figure 6 is a schematic diagram of the proposed remote phosphor QD prism film inside a LCD backlight. The QD prism film consists of a uniform QD layer and two thin substrates. Green and red QD nanoparticles are evenly distributed inside the QD layer. The input surface of the bottom substrate is covered with an array of microprisms. Grooves are parallel to LGP's input edge. The input microprism cross section is

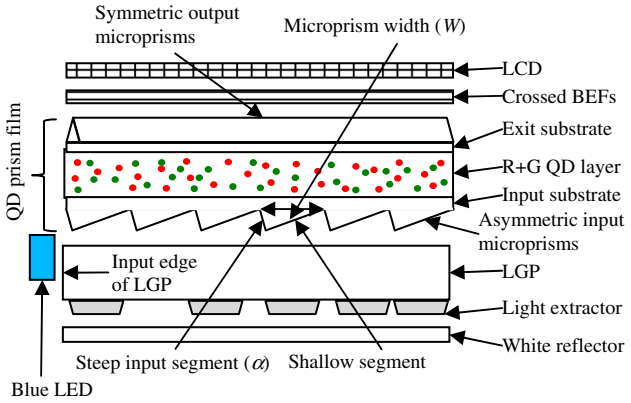

Fig. 6. LCD backlight using the proposed QD prism film having microprism arrays on the surfaces of the top and bottom substrates.

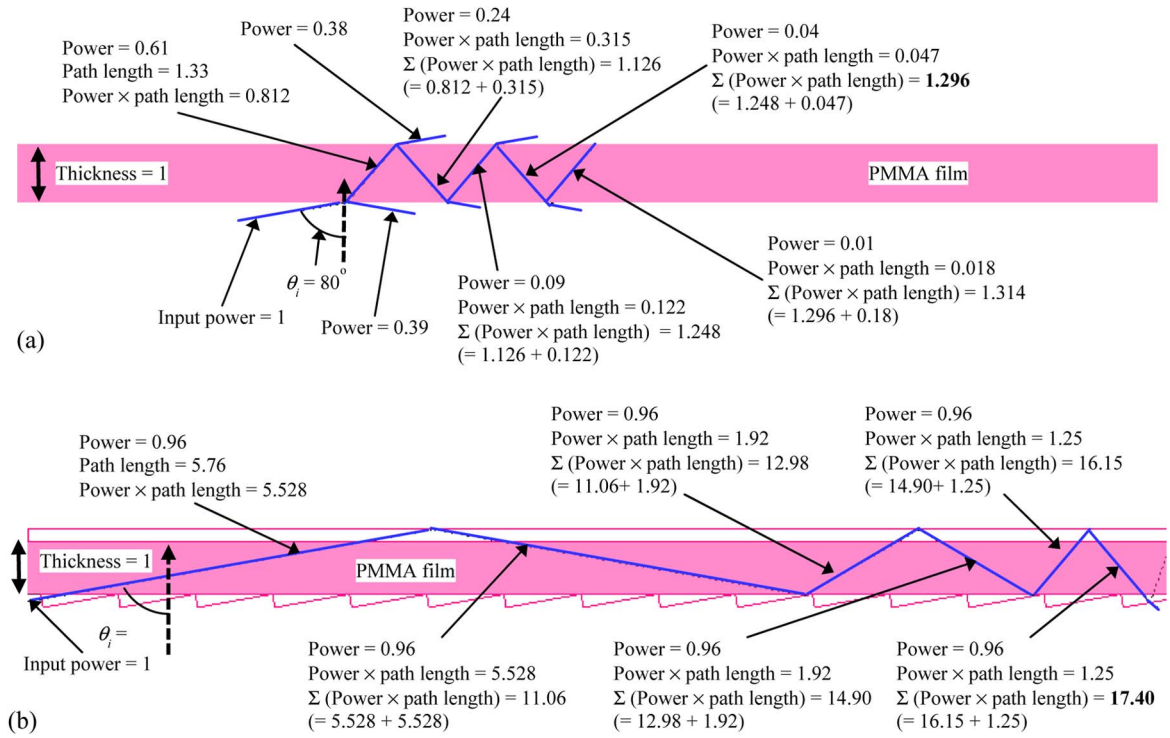

Fig. 7. Tracing of a light ray inside (a) a reference PMMA film with planar optical surfaces on top and bottom, and (b) a PMMA film with arrays of asymmetric microprisms on the input surface and symmetric microprisms on the exit surface. The tilt angle is 80° for the bottom prisms' steep input segment and 10° for the shallow segment. Symmetric output prisms have a 90° included angle. The output prisms' grooves are perpendicular to the input prisms. PMMA's refractive index is 1.5003 at $\lambda = 459$ nm.

asymmetric, and the included angle is 90°. The steep input segment (α) tilts at 80° to preserve the large traveling angle of the off-axis incident light. The input microprism width (W) is 50 μm and the height is 8.5 μm. The bottom substrate's refractive index matches the QD layer's refractive index to avoid TIR on the planar interface. To further increase the reflectance on the top substrate and trap more blue light inside the QD film for downconversion, the top substrate's exit surface is covered with output microprisms. The angle of the symmetric cross section is also 90°, but the grooves are orthogonal to the input prisms. The output microprism's width is 50 μm and the height is 25 μm. To simplify our analysis, we assume the substrates and QD matrix are PMMA material. We use LightTools' default interpolation coefficients for refractive index and the default transmittance/length for absorption.

Figures 7(a) and 7(b) reveal the working mechanism of the proposed surface microprisms. Figure 7(a) traces the power of a light ray inside a reference PMMA film at 80° incident angle; here, both the input and exit surfaces are planar optical surfaces. Transmittance on the planar optical surface determines that only 61% of incident blue light can enter the PMMA film; the remaining 39% is reflected back. According to Snell's law, the light's angle becomes 41° off-axis inside the PMMA film. Thus, the light's traveling distance is 1.33× the film's thickness before it reaches the exit surface. As discussed above, QD film has higher optical efficiency if a higher percentage of incident light travels a longer distance inside the QD layer. To take into account both power and path length, we accumulate the multiplication of the light ray's power (∅) and path length (d), which is $\sum(\varnothing \times d)$. The first $(\varnothing \times d)$ is $0.61 \times 1.33 = 0.812$. After bouncing between the input and exit surfaces five times, the light ray's power drops to 1% and $\sum(\varnothing \times d)$ barely increases to 1.314.

Figure 7(b) shows that the PMMA film has asymmetric microprisms on the input surface and symmetric microprisms on the exit surface. The tilted input segment is normal to the incident light. About 96% of the incident light travels into the PMMA film without losing the large angle. Traveling distance is increased to 5.76 before hitting the exit surface. The first $(\varnothing \times d)$ becomes 5.528. Then all of the blue light is reflected back because of TIR on the output microprisms. The power and path length are not changed so that $\sum(\varnothing \times d)$ is doubled to 11.06. When the reflected light hits the shallow segment of the input microprism, the TIR condition is still satisfied. However, the reflected light is folded back toward on-axis each time it hits one of the shallow segments. The light continues to bounce between the input and exit surfaces six times until the TIR condition is not satisfied. This increases $\sum(\varnothing \times d)$ to 17.4. That is 13.2× higher than the $\sum(\varnothing \times d)$ produced by the reference PMMA film. The proposed microprisms allow a larger portion of incident blue light to enter the film and travel a longer distance inside the film. Once the film is filled with QD particles, downconversion occurs at much higher efficiency due to the excitation light's higher power and increased probability of hitting QD particles. At the same time, the microprisms' slanted surfaces extract the re-emitted lights beyond

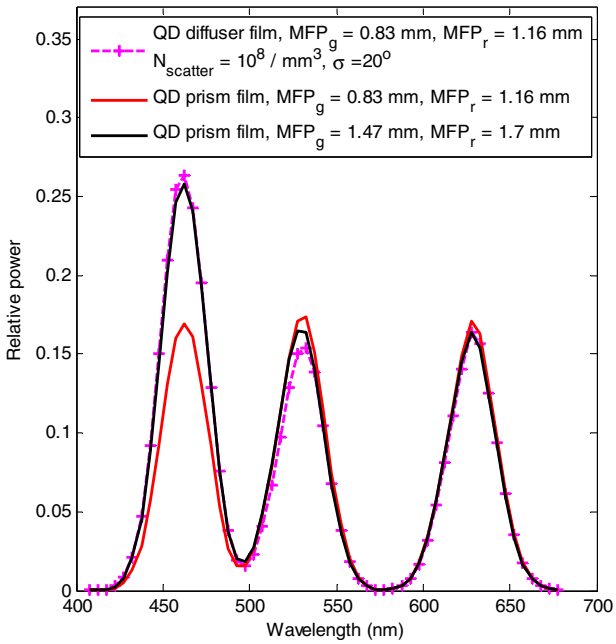

Fig. 8. Relative power spectra of the outputs from the proposed QD prism film and a conventional QD diffuser film. For QD prism film, the tilt angle of the steep input segment is 80° and the prism width is 50 μm. Conventional QD diffuser film has scattering particle density $N_s = 10^8/\text{mm}^3$ and surface scattering $\sigma = 20°$. QD layer thickness = 200 μm.

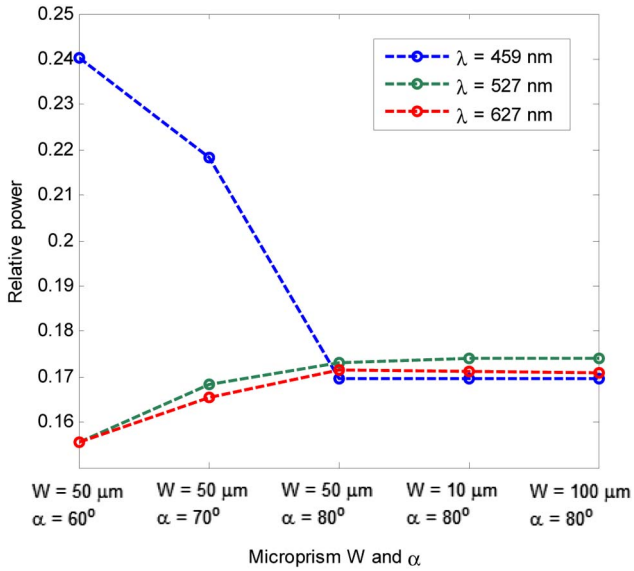

Fig. 9. Peaks of the relative powers at blue, green, and red spectra when the input segment tilt angle (α) increases from 60° to 80°, while the microprism width is fixed at $W = 50$ μm. After that, the tilt angle (α) is fixed at 80°, but with much smaller width, $W = 10$ μm, later using much larger width, $W = 100$ μm. Here MFP_g is fixed at 0.83 mm and $\text{MFP}_r = 1.16$ mm.

the light emission cone by folding the light rays toward the on-axis.

The above analyses can be validated by LightTools' ray-tracing simulation. Comparing the red solid line with the pink dashed lines in Fig. 8, we find that, using the same amount of green and red QDs and no volume scattering particle at all, the proposed QD prism film absorbs much more blue light and re-emits higher power green and red light than conventional diffusive QD film. The relative peak of the blue spectrum is reduced from 0.263 to 0.17, while the green and red light increase from 0.15 and 0.164 to 0.171. Here we assume $\text{MFP}_g = 0.83$ mm and $\text{MFP}_r = 1.16$ mm for both QD films. The steep input segment of the input microprism is tilted at 80° and the angle of the shallow segment is 10°. The microprism width is 50 mm. Conventional diffusive QD film has volume scattering particle $N_s = 10^8/\text{mm}^3$ and surface scattering $\sigma = 20°$. The proposed surface microprisms are so effective in improving the QD film's optical efficiency, eventually much less QD material is required to maintain strong downconversion, as the black line in Fig. 8 demonstrates. After increasing MFP_g to 1.47 mm and MFP_r to 1.7 mm, the power of re-emitted light stays higher, and the power of unabsorbed blue light remains lower, compared to the outputs of QD diffuser film. That is 58% longer MFP_g and 35% longer MFP_r, implying 58% saving in green QD and 35% in red QD materials.

Because the input surface's microprism array is designed to couple the incident light and preserve the large off-axis angle, the tilt angle of the microprism input segment is more important than microprism width. Figure 9 compares the peak power in blue, green, and red spectra at different tilt angles (α) of the steep input segment and different widths (W) of the input microprism. With the fixed width $W = 50$ μm, increasing tilt angle α from 60° to 80° reduces blue light's relative peak power from 0.24 to 0.17, and increases green's and red's relative peak powers by more than 10%. Therefore, a steeper input segment is preferred. In contrast, the output spectra are barely changed when the input microprism width is reduced to a much smaller size, $W = 10$ μm, or doubled to 100 μm. This provides us a wide choice in microprism dimensions as long as it is large enough to avoid light scattering and small enough to avoid being visible to the human eye [21]. The output surface's retro-reflective microprisms have similar requirements for dimensions, except that the microprisms' surfaces are tilted at 45° to reflect back the incident light, as previously discussed in Fig. 7.

To minimize backlight power consumption at the same time to ensure that the LC panel is capable of producing a white image, there is a preferred range of the ratios among blue, green, and red components [4,5]. Higher power in the blue region is desired for LCD backlights to offset the LC panel's relatively stronger absorption in shorter wavelengths. The ratio between the remaining blue light and the re-emitted green and red light can be fine-tuned by adjusting QD particle densities. The solid lines in Fig. 10 compare the peak powers in the blue, green, and red spectra when MFP_g is increased from 0.63 to 1.23 mm and MFP_r is between 0.96 and 1.56 mm, in increments of 0.1 mm. A decrease in blue light power from 0.235 to 0.133 suggests that the absorption of blue light increases significantly when the QD MFP decreases, or QD particle density increases. While the powers of the green and red spectra peak at $\text{MFP}_g = 0.83$ mm and $\text{MFP}_r = 1.16$ mm, increasing or

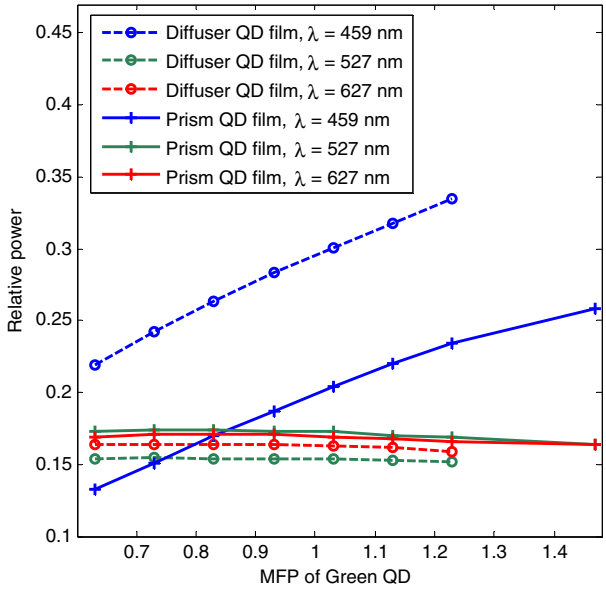

Fig. 10. Peaks of the relative powers at the blue, green, and red regions when MFP_g increases from 0.63 to 1.23 mm in 0.1 mm increments and MFP_r is between 0.96 and 1.56 mm. The output spectra of the proposed QD prism film with $MFP_g = 1.47$ mm and $MFP_r = 1.7$ mm in Fig. 8 are repeated. Conventional diffusive QD film has scattering particle density $N_s = 10^8/\text{mm}^3$ and surface scattering $\sigma = 20°$. QD layer thickness = 200 μm.

decreasing the QD MFP only reduces the output. This can be explained by QD secondary absorption. The dashed lines in Fig. 10 illustrate similar trends for conventional diffusive QD film. However, the power of re-emitted light is lower, even lower than the light outputs produced by the proposed QD prism film at much larger MFPs, while the remaining blue light has much higher power. Too much blue component is also problematic. Instead of packing a lot more QD particles or taking extra effort to handle the redundant blue light, QD prism film is significantly more effective in converting blue light to green and red light, which means using much less QD material and packing at much lower density to achieve the preferred output spectra and higher optical efficiency.

4. CONCLUSION

We developed a highly efficient remote phosphor QD prism film for edge-lit LCD backlights. The proposed configuration extends the blue light optical path inside the QD layer and significantly increases the downconversion efficiency. Without any volume scattering particle, the proposed prism film uses less QD material to absorb more blue light and re-emit higher power green and red light. Lower particle density further improves the optical efficiency through reducing QD aggregation. This design also helps to reduce the QD material cost. Low-cost manufacturing of microprism substrates is commonly available for the display optical film industry. By using less of still expensive QD material and no scattering particles, the proposed QD backlight is more affordable and can be more competitive for both small-size portable displays and large-screen LCD TVs.

Industrial Technology Research Institute (Taiwan).

The authors are indebted to Dr. Yajie Dong for valuable discussion.

REFERENCES

1. S. Coe-Sullivan, P. Allen, and J. S. Steckel, "Quantum dots for LED downconversion in display applications," ECS J. Solid State Sci. Technol. **2**, 3026–3030 (2013).
2. J. Chen, V. Hardev, J. Hartlove, J. Hofler, and E. Lee, "A high-efficiency wide-color-gamut solid-state backlight system for LCDs using quantum dot enhancement film," SID Symp. Dig. Tech. Papers **43**, 895–896 (2012).
3. E. Jang, S. Jun, H. Jang, J. Lim, B. Kim, and Y. Kim, "White-light-emitting diodes with quantum dot color converters for display backlights," Adv. Mater. **22**, 3076–3080 (2010).
4. Z. Luo, D. Xu, and S. T. Wu, "Emerging quantum-dots-enhanced LCDs," J. Disp. Technol. **10**, 526–539 (2014).
5. Z. Luo, Y. Chen, and S. T. Wu, "Wide color gamut LCD with a quantum dot backlight," Opt. Express **21**, 26269–26284 (2013).
6. T. Erdem, S. Nizamoglu, X. W. Sun, and H. V. Demir, "A photometric investigation of ultra-efficient LEDs with high color rendering index and high luminous efficacy employing nanocrystal quantum dot luminophores," Opt. Express **18**, 340–347 (2010).
7. P. Zhong, G. X. He, and M. H. Zhang, "Optimal spectra of white light-emitting diodes using quantum dot nanophosphors," Opt. Express **20**, 9122–9134 (2012).
8. J. S. Steckel, R. Colby, W. Liu, K. Hutchinson, C. Breen, J. Ritter, and S. Coe-Sullivan, "Quantum dot manufacturing requirements for the high volume LCD market," SID Symp. Dig. Tech. Papers **44**, 943–945 (2013).
9. I. H. Campbell and B. K. Crone, "Efficient, visible organic light-emitting diodes utilizing a single polymer layer doped with quantum dots," Appl. Phys. Lett. **92**, 043303 (2008).
10. S. Coe-Sullivan, "Quantum dot developments," Nat. Photonics **3**, 315–316 (2009).
11. H. Kim, H. Hong, C. Yoon, H. Choi, I. Ahn, D. Lee, Y. Kim, and K. Lee, "Fabrication of high quantum yield quantum dot/polymer films by enhancing dispersion of quantum dots using silica particles," J. Colloid Interface Sci. **393**, 74–79 (2013).
12. O. O. Matvienko, Y. N. Savin, A. S. Kryzhanovska, O. M. Vovk, M. V. Dobrotvorska, N. V. Pogorelova, and V. V. Vashchenko, "Dispersion and aggregation of quantum dots in polymer–inorganic hybrid films," Thin Solid Films **537**, 226–230 (2013).
13. L. Qian, Y. Zheng, J. Xue, and P. H. Holloway, "Stable and efficient quantum-dot light-emitting diodes based on solution-processed multilayer structures," Nat. Photonics **5**, 543–548 (2011).
14. B. S. Mashford, M. Stevenson, Z. Popovic, C. Hamilton, Z. Q. Zhou, C. Breen, J. Steckel, V. Bulovic, M. Bawendi, S. Coe-Sullivan, and P. T. Kazlas, "High-efficiency quantum-dot light-emitting devices with enhanced charge injection," Nat. Photonics **7**, 407–412 (2013).
15. S. Kim, S. H. Im, and S. W. Kim, "Performance of light-emitting-diode based on quantum dots," Nanoscale **5**, 5205–5214 (2013).
16. A. Castan, H.-M. Kim, and J. Jang, "All-solution-processed inverted quantum-dot light-emitting diodes," ACS Appl. Mater. Interfaces **6**, 2508–2515 (2014).
17. K. Cho, E. Lee, W. Joo, E. Jang, T. Kim, S. Lee, S. Kwon, J. Han, B. Kim, B. Choi, and J. Kim, "High-performance crosslinked colloidal quantum-dot light-emitting diodes," Nat. Photonics **3**, 341–345 (2009).
18. J. Lim, W. K. Bae, J. Kwak, S. Lee, C. Lee, and K. Char, "Perspective on synthesis, device structures, and printing processes for quantum dot displays," Opt. Mater. Express **2**, 594–628 (2012).
19. Y. Shirasaki, G. J. Supran, M. G. Bawendi, and V. Bulovic, "Emergence of colloidal quantum-dot light-emitting technologies," Nat. Photonics **7**, 13–23 (2013).
20. M. Zollers, "Phosphor modeling in LightTools," LightTools White Paper, 2011, http://optics.synopsys.com/lighttools/pdfs/ModelingPhosphorsInLightTools.pdf.
21. H. C. van de Hulst, *Light Scattering by Small Particles* (Wiley, 1957).